All-cellulose Composites Fabricated by *in-situ* Welding

Meixue Gan,[a] Lang Tian,[a] Yiruo Chen,[a] Jieting Xin,[a] Hui Si,[b,*] Yimin Xie,[a] and Qinghua Feng [a,c,*]

As a consequence of increasingly serious environmental problems, many researchers are highlighting biomass materials. Cellulose, the most abundant bioresource, is becoming a key consideration for alleviating environmental pollution. Characterization of cellulosic materials is fundamental to exploring their structures and elemental contents. Scanning electron microscopy (SEM) and X-ray diffraction (XRD) are frequently employed to study the structure of cellulose. Thus, it is urgent to combine traditional means with new ones. This study focused on the characterization of the all-cellulose composites (ACCs) model prepared *via* partially dissolving filter paper using 40% benzyltrimethylammonium hydroxide ($BzMe_3NOH$) aqueous solution. Characterized by SEM, XRD, Fourier transformation infrared spectroscopy, Raman spectroscopy, and X-ray photoelectron spectroscopy, the unique transformation from cellulose I to cellulose II of the ACCs model was explored. These characterization methods exhibited respective features, which could be universal ways to investigate ACCs.

DOI: 10.15376/biores.18.2.3044-3055

Keywords: All-cellulose composites; Cellulose I/II; Micro/nano-fiber

*Contact information: a: Hubei Provincial Key Laboratory of Green Materials for Light Industry, New Materials and Green Manufacturing Talent Introduction and Innovation Demonstration Base, Hubei University of Technology, Wuhan 430068, China; b: Technology R&D Center, China Tobacco Hubei Industrial Corporation, Wuhan, 430040, China; c: Key Laboratory of Pulp and Paper Science and Technology of Ministry of Education, Qilu University of Technology (Shandong Academy of Sciences), Jinan 250353, China; *Corresponding authors: sihui@hbtobacco.cn; fqhpaper@163.com*

INTRODUCTION

With the rapid development of science and technology, cellulose-based materials are becoming increasingly important because of their easy characterizations and improved applicability. Cellulose, an important part of plants, is the oldest and most abundant natural polymer on the earth (Baghaei and Skrifvars 2020; Li *et al.* 2021). Because of its natural degradability and renewable nature, cellulose is considered to be an inexhaustible and valuable renewable biomass resource (Xia *et al.* 2021), which could be utilized in many advanced areas, *e.g.*, smart materials (Zhao *et al.* 2022) and exhibiting different crystal forms under different treatments. Up to now, the known cellulose crystal types are cellulose I, cellulose II, cellulose III, and cellulose IV (Agarwal *et al.* 2021). Especially cellulose II is usually formed during many laboratory and industrial processes when treated using N-methylmorpholine-N-oxide (NMMO) (Rosenau *et al.* 2001), ionic liquid (Duchemin *et al.* 2009; Reyes *et al.* 2019), lithium chloride/N,N-dimethylacetamide (LiCl/DMAc) (Pullawan *et al.* 2014; Zhao *et al.* 2014), tetrabutylphosphonium hydroxide aqueous solution (TBPH) (Baranov *et al.* 2021), aqueous tetraethylammonium hydroxide solution (TEAOH) (Sirviö *et al.* 2017), sodium hydroxide/urea (NaOH/urea) aqueous solvent

(Xiong *et al.* 2014; Shi *et al.* 2015), NaOH/urea/ZnO solution (Jiao *et al.* 2015), *etc*. Following the trend of reducing the consumption of traditional plastics, researchers have set their sights on all cellulose composites (ACCs), which can have excellent degradability, outstanding renewability, environment-friendly nature, nontoxicity, and tunable strength. Over the past few years, a lot of cellulose-based materials have been extensively studied. For example, Labidi *et al.* (2019) used alfa and wood fibers to fabricate good mechanical performance ACCs, resulting in the Young's modulus of 3.8 GPa (based on alfa) and 4.2 GPa (based on wood). Xie *et al.* (2020) employed cellulose to produce the cellulosic paper with excellent oil and grease resistance *via* NaOH/urea aqueous solution, which could be used in food packing. An antibacterial material was prepared by Ma *et al.* (2016) using partially dissolved cellulose with zinc oxide in a special package because of its mold resistance. A lot of ACCs materials have been presented, although the characterization analysis methods are still not impeccable. Traditional characterization analysis of cellulose or cellulosic composites generally depends on X-ray diffraction (XRD), Fourier transformation infrared (FT-IR) spectroscopy, and scanning electron microscopy (SEM). In addition, it is possible to combine the data explored by new methods (Raman and X-ray photoelectron (XPS) spectroscopies) at the same time (Duchemin *et al.* 2009, 2016; Montoya-Rojo *et al.* 2021).

In this paper, the authors expanded the traditional characterization system and added two new characterization methods. The ACCs prepared through a one-step method were explored by the transfer of the crystal conditions *via* SEM, XRD, FT-IR, Raman spectroscopy, and XPS. Thus, a comprehensive analysis was conducted. Through the experiment, the changes from raw sample to resulting product sample were confirmed.

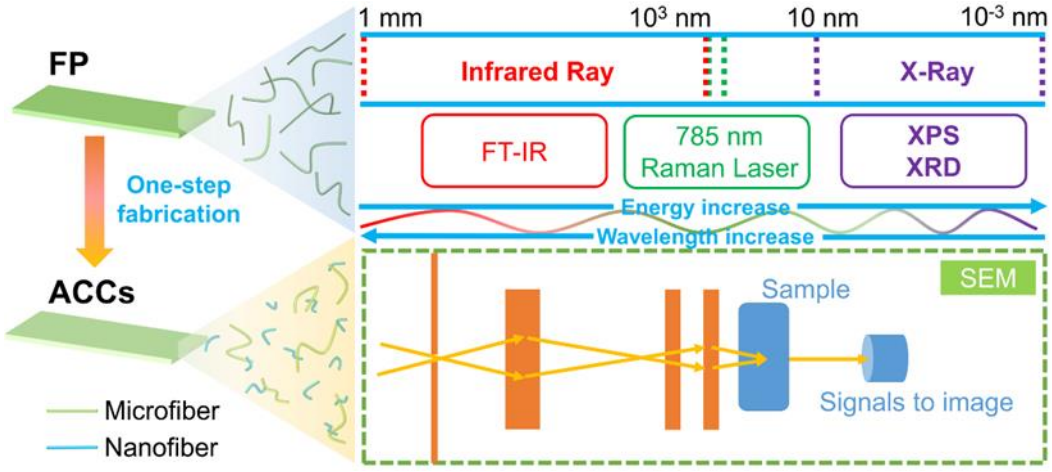

Fig. 1. The structural determinations of FP and ACCs

EXPERIMENTAL

Materials

Double circle qualitative filter paper (FP, made from cotton fiber) with a diameter of 18 cm and 40 wt% benzyl trimethylammonium hydroxide aqueous solution was purchased from General Electric Biotechnology Co., Ltd. (Hangzhou, China) and TCI

Shanghai Co., Ltd. (Shanghai, China), respectively. All other chemical reagents were analytical grade and used directly without further purification prior to use.

Preparation of FP-treated with $BzMe_3NOH$ Aqueous Solution

The FP with strength not exceeding ± 0.5 N was first screened, and the round FP was cut into a rectangle (4.5 × 15 cm^2). Next, the cut FP was impregnated in $BzMe_3NOH$ aqueous solution (10%, 20%, 30%, and 40%) for 1.0 s at 8 °C. Based on a comparison of different weights before and after immersing in solvents, the FP absorbed 240 ± 10 $g \cdot m^{-2}$ of $BzMe_3NOH$ aqueous solution. Then, the impregnated FP was immediately stored in a refrigerator (8 °C) for 0 s, 15 s, 30 s, 60 s, 120 s, 300 s, and 600 s. After that, the FP was washed with deionized water at room temperature for a few days to replace $BzMe_3NOH$. Finally, the ACCs were dried in the dryer section of the Rapid-Köthen paper former (RK-3A, PTI, Vorchdorf, Austria) for 15 min (95 °C, 10 kPa). The obtained treated FP was ACCs, including FP8-x and FP8-y (x is the dissolve time, including 0 s, 15 s, 30 s, 60 s, 120 s, 240 s, 300 s, and 600 s; y is the concentration, including 10%, 20%, 30%, and 40%). All materials were placed in a constant temperature and humidity room at 23 °C and 50% relative humidity (RH) for at least 24 h for structural determinations (Fig. 1) and mechanical strength tests.

SEM Analysis

Morphology analysis of FP and ACCs (after drying) in cross-section and surface was carried out with imaging by an ultra-high resolution cold field scanning electron microscope (SU8010, HITACHI Ltd., Tokyo, Japan) with a 5 kV accelerating voltage. To enhance the electric conductivity, the FP and ACCs were sprayed with gold using a SEM sputtering coater (MC1000; HITACHI Ltd., Tokyo, Japan). For cross-sectional images, the samples were prepared by cutting with a utility knife or freeze-drying (treated in *tertiary*-butyl alcohol).

XRD Analysis

The crystallization structures of FP and ACCs cut into slices (1.5 × 1.5 cm^2) were determined and collected by X-ray diffraction (Empyrean, PANalytical B.V., Almelo, Netherlands) equipped with a CuKα (k = 1.54 A°) monochromatic radiation source with a wavelength of 0.154 nm, 45 kV operating tube voltage, and 40 mA tube current. All the diffracted intensities from 5° to 40° were recorded with a step size of 0.05° using reflection mode. Then, the XRD patterns were presented after eliminating excess noise and removing the environmental background.

XPS Analysis

Surface chemical analysis of FP and ACCs samples was performed using an X-ray photoelectron spectrometer (PHI5000 Versaprobe III XPS, Physical Electronics, Inc., Chanhassen, MN, USA) equipped with Al Kα radiation as the excitation resource.

FT-IR Spectroscopy and Raman Spectroscopy

Fourier transform-infrared spectra (Nicolet 6700 FT-IR, Thermo Fisher Scientific Inc., Waltham, MA, USA) with an ITR Attenuated Total Reflectance (ATR) diamond and Raman spectra (XploRA™ PLUS, Horiba, Ltd., Kyoto, Japan) were employed to obtain molecular information of FP and ACCs. The confocal Raman instrument was also used to record the images of FP and ACCs (785 nm light at 30 mW power and 50X objective, NA

0.90). The FT-IR and Raman spectra were recorded in the 4000 to 650 cm^{-1} and 1500 to 300 cm^{-1} regions, respectively.

Tensile Tests

An electromechanical universal testing machine (1.0 kN load cell) (CMT6103, MTS Industrial Systems Co., Ltd., Shenzhen, China) was used to test the mechanical properties of ACCs and FP (15 × 100 mm^2, 10 mm min^{-1}), and all the tests were performed at a room condition (25 °C, 50% RH). Further, the thickness of FP and ACCs was the average value of five random measurement points using a thickness gauge (DC-HJY03; Sichuan Changjiang Papermaking Instrument Co., Ltd., Yibin, China).

RESULTS AND DISCUSSION

Micromorphology and Crystal Type Analysis

The morphology of ACCs was examined through SEM (Fig. 2). The pictures show visible differences when comparing before and after solvent treatment. As shown in Figs. 2(b) and (B), the ACCs seemed to have smaller apertures than the FP. Figure 2(b) shows a lot of microfibers that are entangled in the surface image of FP. Moreover, compared with the FP, the ACCs underwent some transformation. It can be directly perceived that a lot of nanocellulose fibers were present on the surface and the cross-section of ACCs, constituting the unique intertwined structure of microfibers and nanofibers (Yousefi *et al.* 2015; Hu *et al.* 2021b; Nemoto and Nakamata 2021; Bian *et al.* 2022; Yu *et al.* 2022).

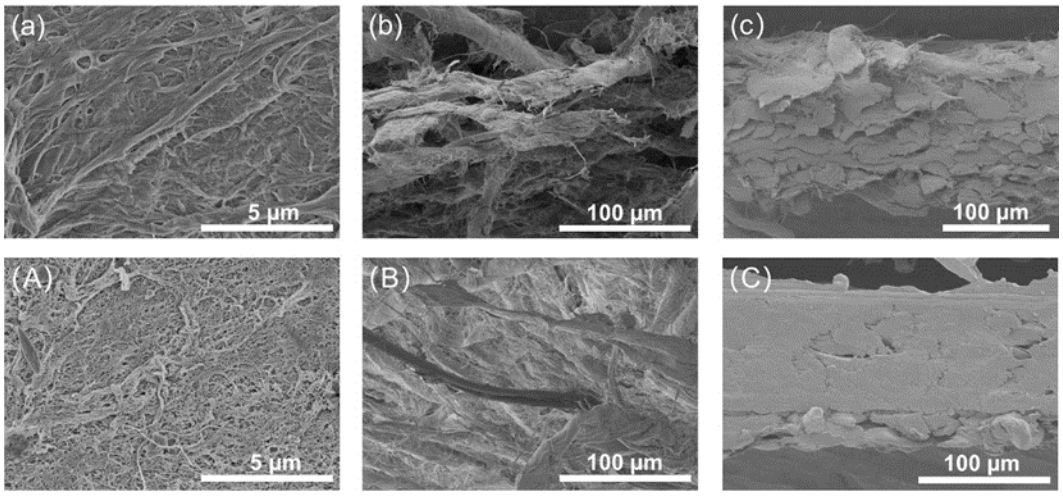

Fig. 2. The SEM pictures of ACCs (uppercase letters) and FP (lowercase letters): (A), (a): The SEM images of the surface; (B), (b): The SEM images of brittle fracture cross-section; and (C), (c): The SEM images of the cross-section cut with a utility knife

Moreover, the cross-section surfaces of FP and ACCs (Figs. 2(c) and (C)) could suggest that the ACCs had a smaller fiber diameter than FP. This means that the amorphous areas of P and S1 walls of the fibers were partially swelled and dissolved (Tang *et al.* 2021). As revealed in Figs. 2(a) and (A), the FP showed a common structure of fibers (Fig. 2(a)), while the fracture structure of ACCs was relatively denser and smoother due to the *in-situ* welding of fibers through cellulose matrix (Fig. 2(A)). These results indicate that FP treated

by $BzMe_3NOH$ aqueous solution formed a composite structure of microfibers and nanofibers, *i.e.*, ACCs (Hu *et al.* 2021a).

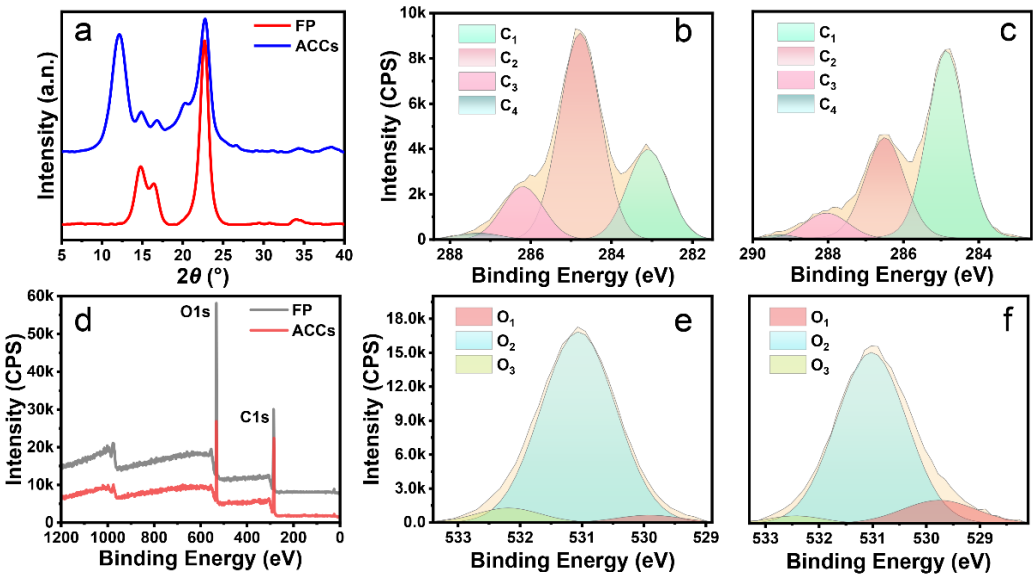

Fig. 3. (a) XRD spectra of FP and ACCs; (b) C1s spectra of FP; (c) C1s spectra of ACCs; (d) XPS survey of FP and ACCs; (e) O1s spectra of FP; and (f) O1s spectra of ACCs

Table 1. O/C Ratio and Carbon Contents of FP and ACCs*

Sample	O/C	Content (%)			
		C1	C2	C3	C4
Untreated	0.71	25.29	57.93	14.86	1.92
Treated	0.41	57.69	32.69	8.72	0.90

*Calculated summary of XPS spectral parameters of all sheets by fitting

Furthermore, the crystalline compositions of FP and ACCs were characterized by XRD (Fig. 3(a)). The figure illustrates that the structure of FP had great changes after treatment. There were obvious characteristic peaks in Fig. 3(a), and it is clear that the FP showed strong absorption peaks around 14.7°, 16.4°, 22.6°, and 34.4°, representing the (1-10), (110), (200), and (004) crystallographic planes of cellulose I, respectively (Sebe *et al.* 2012; Zhu *et al.* 2017; Hu *et al.* 2020; Hu *et al.* 2021a,b; Bian *et al.* 2022). Excluding the peaks of primary peaks of cellulose I (14.7°, 16.4°, 22.2°, and 34.4°), the ACCs showed a high additional absorption peak around 12.2° and a relatively obvious peak around 20.2°, corresponding to the (1-10) and (110) crystallographic planes of cellulose II, respectively (Wang *et al.* 2019; Hu *et al.* 2021a, 2021b; Bian *et al.* 2022). Their findings could confirm that microfibers and nanofibers simultaneously were present in the ACCs.

XPS Analysis

Surface chemical composition could also reflect the changes from FP to ACCs. Figure 3(d) shows the dominating peaks of carbon and oxygen but does not show nitrogen, indicating that there was no residual solvent in the processed sample. Herein, the signals

from C1s region were made into 4 peaks based on the literature. The four peaks represented by C1−C4 correspond to C−C and/or C−H (C1), C−O (C2), C=O, and/or O−C−O (C3), and O=C−O (C4) (Sebe *et al.* 2012; Wang *et al.* 2019; Hu *et al.* 2021a, 2021b; Bian *et al.* 2022).

As shown in the C1s spectra (Figs. 3(b) and (c)), there was an increase of C1 and decrease of C2 contents, which could indicate that there are fewer hydroxyl groups on the surface of ACCs than that on the surface of FP because of the transformation from cellulose I to cellulose II (Hao *et al.* 2019; Hu *et al.* 2021a; Yu *et al.* 2022). Moreover, the O/C ratio also changed (Table 1). Compared with the O/C ratio of ACCs (0.41), the value of FP (0.71) was higher. The reason for this phenomenon is also because of the reduction of surface hydroxyl number before and after treatment (from cellulose I to cellulose II). In the three peaks represented by O1−O3, compared to Figs. 3(e) and 3(f), the content of O2 (C–O–, C=O, C–O–C, O–C=O) of ACCs increased, while the content of O1 (C–O) decreased. This may mean that less hydroxyl was exposed on the surface of ACCs compared to FP. These results could further confirm the transformation from cellulose I to cellulose II.

FT-IR Spectroscopy

The FT-IR spectroscopy was used to characterize crystalline patterns based on the conformation of the C(6) group (Nelson and O'Connor 1964b; Lee *et al.* 2013; Duchemin *et al.* 2016; Hu *et al.* 2021a). Through the FT-IR spectra, many absorbance peaks of FP could be observed. Figure 4(d) shows the major peaks at 3330, 2895, 1640, 1365, and 1030 cm^{-1}. The wide peaks of 3330 cm^{-1} are associated with O−H stretching vibration in the cellulose (Oh *et al.* 2005; Lourdin *et al.* 2015; Duchemin *et al.* 2016; Almeida *et al.* 2020; Xi *et al.* 2021; Bian *et al.* 2022). The absorbance peaks at 2895 and 1640 cm^{-1} respectively, correspond to C−H stretching and C=O stretching vibrations (Oh *et al.* 2005; Duchemin *et al.* 2016). Furthermore, the peaks around 1365 and 1030 cm^{-1} could illustrate C−H bending and C−O stretching vibrations from cellulose (Nelson and O'Connor 1964a; Lourdin *et al.* 2015; Duchemin *et al.* 2016). It is more important that the absorption peaks of 897 cm^{-1} intensity increase and shift to 894 cm^{-1}, which may suggest the transformation of cellulose crystalline patterns (Oh *et al.* 2005; Hu *et al.* 2021a). It could also be found that the peaks at 3330 cm^{-1} appear as two shoulder peaks at 3447 and 3480 cm^{-1}. Symmetric CH_2 bending or scissoring motions are relevant to the change in the peak from 1427 to 1417 cm^{-1}, which indicates that during the ACCs preparation process cellulose I was transformed to cellulose II (Nelson and O'Connor 1964a; Carrillo *et al.* 2004; Oh *et al.* 2005; Duchemin *et al.* 2016; Hu *et al.* 2021a; Bian *et al.* 2022).

Raman Spectroscopy

The analysis of crystalline structure changes could be achieved by Raman spectroscopy. The Raman spectra (in the range of 300 to 1500 cm^{-1}) of FP and ACCs are shown in Fig. 4(c). Despite the lower resolution of Raman, the variation of multiple bands can also detect polymorphic changes between 300 and 1500 cm^{-1} (Hu *et al.* 2021a). From the spectra, it could be noted that the appearance of a new spectral peak at 577 cm^{-1} corresponds to the typical bond in cellulose II. Moreover, the band intensity at 1472 cm^{-1}, assigned as the CH_2 and H-O-C bending and CH_2 in-plane scissoring, increased (Fischer *et al.* 2005; Schenzel *et al.* 2005; Hettrich *et al.* 2014; Agarwal *et al.* 2021). The peak at 897 cm^{-1} assigned as the bending mode for H-C-C and H-C-O at C(6) increased (Schenzel and Fischer 2001; Hu *et al.* 2021a). Furthermore, the bands at 330, 900, and 1472 cm^{-1} increased, and the bands at 458 cm^{-1}, 519 cm^{-1}, and 966 cm^{-1} decreased. These results could

express a part of cellulose I transformation to cellulose II, which is in accordance with XRD, FT-IR, and XPS (Agarwal 2014; Hettrich *et al.* 2014; Agarwal *et al.* 2021; Hu *et al.* 2021a, 2021b).

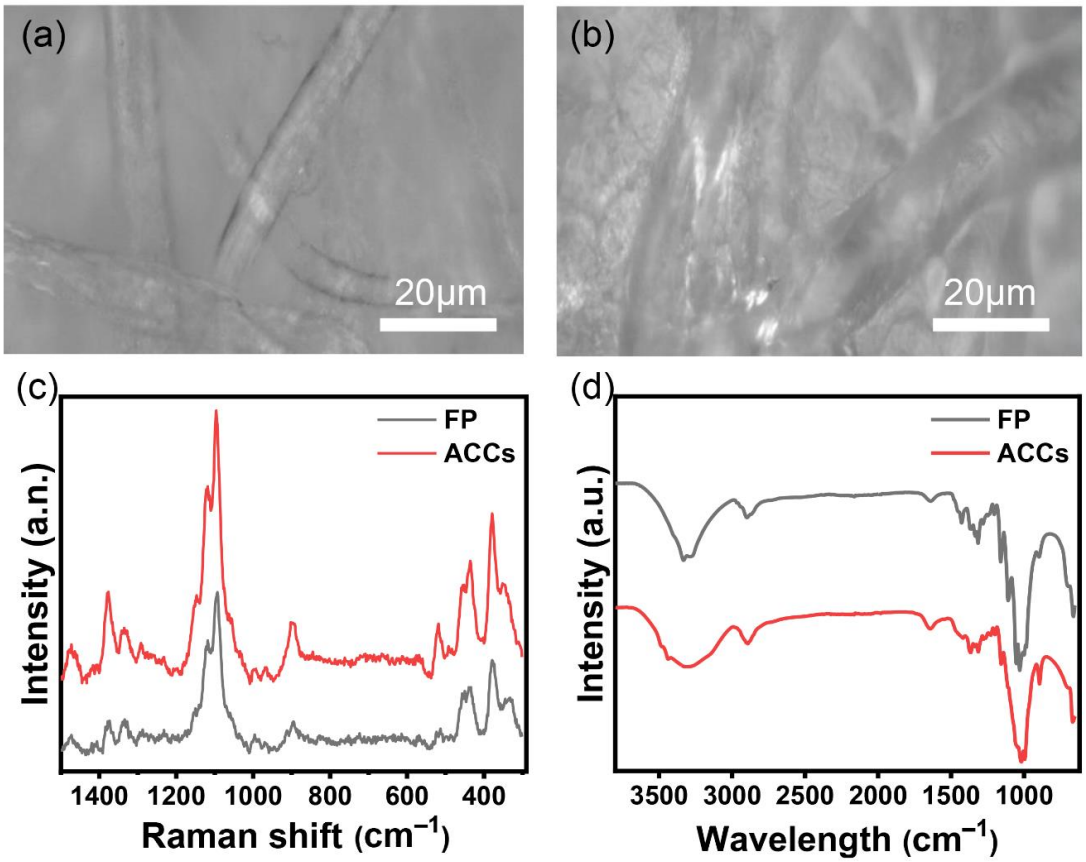

Fig. 4. Raman optical microscopic images of FP (a); ACCs (b); (c) Raman spectra of FP and ACCs; and (d) FT-IR spectra of FP and ACCs.

Tensile Tests

The mechanical properties were explored by the stress-strain curves of FP and ACCs (Fig. 5). It could also be found that lower concentration (10% to 20%) had a side effect on the mechanical strength of samples, which could reduce their mechanical properties from ~7.89 to ~6.50 MPa (FP8-10%) and ~7.15 MPa (FP8-20%) (Fig. 5(a)). Nevertheless, FP treated by relatively high concentrations (FP8-30% and FP8-40%) exhibited an increased tensile strength of ~10.19 MPa (FP8-30%) and ~19.91 MPa (FP8-40%). Moreover, the ACCs prepared in a short time or long time could both obtain an excellent performance (Fig. 5(b)), demonstrating that time had less effect on the strength of ACCs. The mechanical strength of ACCs increased from 7.89 MPa to 19.90 to 26.41 MPa, which is 2.5 to 3.4 times stronger than FP. In addition, the density of ACCs had some differences in different conditions of time and concentration. As shown in Table 2, with the increase in concentration and the passage of time, the density of ACCs showed a trend of increasing.

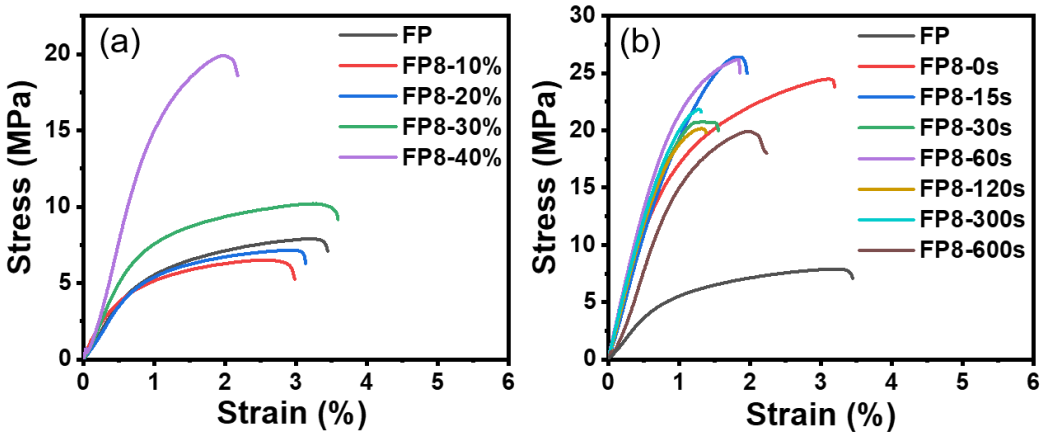

Fig. 5. (a) The stress-strain curves of FP treated with different solvent concentrations; and (b) The stress-strain curves of FP stored in a refrigerator at different time

Table 2. The Density of FP and ACCs

Samples*	Density ($g \cdot cm^{-3}$)	Samples**	Density ($g \cdot cm^{-3}$)
FP	0.465 ± 0.0039	FP8-1s	0.582 ± 0.0047
FP8-10%	0.450 ± 0.0040	FP8-15s	0.648 ± 0.0047
FP8-20%	0.453 ± 0.0038	FP8-30s	0.653 ± 0.0045
FP8-30%	0.490 ± 0.0038	FP8-60s	0.667 ± 0.0044
FP8-40%	0.774 ± 0.0038	FP8-120s	0.713 ± 0.0042
—	—	FP8-300s	0.708 ± 0.0041

* The treated time was 120s.
****** The treatment concentration was 40%.

CONCLUSIONS

1. In this work, scanning electron microcopy (SEM), X-ray diffraction (XRD), Fourier transform infrared (FT-IR) spectrometry, Raman spectrometry, and X-ray photoelectron spectroscopy were employed to explore the changes from cellulose I to cellulose II in detail.
2. Benefiting from the XPS and Raman methods, the simultaneous presence of cellulose I and cellulose II could be further confirmed and observed.
3. The results showed that the subtle difference in the data between FP and ACCs could be magnified, which could confirm the presence of micro/nano-structure. The XPS was used to test the surface chemical compositions and Raman was applied to study the bonding situation, facilitating the complete characterization of ACCs.
4. In addition, the presence of cellulose I and cellulose II were also shown by traditional characterization methods, which suggested the feasibility of the new method (XPS and Raman). Thus, this work proposed that the Raman and XPS methods could be the potential probe to explore the structure of ACCs.

ACKNOWLEDGMENTS

The authors are grateful to the National Natural Science Foundation of China (21878070), Hubei Provincial Universities Outstanding Young and Middle-aged Technological Innovation Team Project (T201205), the Foundation of Key Laboratory of Pulp & Paper Science and Technology of Ministry of Education, and Qilu University of Technology (KF201623).

REFERENCES CITED

Agarwal, U. P. (2014). "1064 nm FT-Raman spectroscopy for investigations of plant cell walls and other biomass materials," *Frontiers in Plant Science* 5, article 490. DOI: 10.3389/fpls.2014.00490

Agarwal, U. P., Ralph, S. A., Baez, C., and Reiner, R. S. (2021). "Detection and quantitation of cellulose II by Raman spectroscopy," *Cellulose* 28, 9069-9079. DOI: 10.1007/s10570-021-04124-x

Almeida, A. P., Oliveira, J., Fernandes, S. N., Godinho, M. H., and Canejo, J. P. (2020). "All-cellulose composite membranes for oil microdroplet collection," *Cellulose* 27, 4665-4677. DOI: 10.1007/s10570-020-03077-x

Baghaei, B., and Skrifvars, M. (2020). "All-cellulose composites: A review of recent studies on structure, properties and applications," *Molecules* 25(12), article 2836. DOI: 10.3390/molecules25122836

Baranov, A., Sommerhoff, F., Duchemin, B., Curnow, O., and Staiger, M. P. (2021). "Toward a facile fabrication route for all-cellulose composite laminates *via* partial dissolution in aqueous tetrabutylphosphonium hydroxide solution," *Composites Part A: Applied Science and Manufacturing* 140, article ID 106148. DOI: 10.1016/j.compositesa.2020.106148

Bian, H., Yang, Y., Tu, P., and Chen, J. (2022). "Value-added utilization of wheat straw: From cellulose and cellulose nanofiber to all-cellulose nanocomposite film," *Membranes* 12(5), article 475. DOI: 10.3390/membranes12050475

Carrillo, F., Colom, X., Sunol, J., and Saurina, J. (2004). "Structural FTIR analysis and thermal characterization of lyocell and viscose-type fibers," *European Polymer Journal* 40(9), 2229-2234. DOI: 10.1016/j.eurpolymj.2004.05.003

Duchemin, B., Corre, D. L., Leray, N., Dufresne, A., and Staiger, M. P. (2016). "All-cellulose composites based on microfibrillated cellulose and filter paper *via* a NaOH-urea solvent system," *Cellulose* 23, 593-609. DOI: 10.1007/s10570-015-0835-4

Duchemin, B. J. C., Mathew, A., and Oksman, K. (2009). "All-cellulose composites by partial dissolution in the ionic liquid 1-butyl-3-methylimidazolium chloride," *Composites Part A: Applied Science and Manufacturing* 40(12), 2031-2037. DOI: 10.1016/j.compositesa.2009.09.013

Fischer, S., Schenzel, K., Fischer, K., and Diepenbrock, W. (2005). "Applications of FT Raman spectroscopy and micro spectroscopy characterizing cellulose and cellulosic biomaterials," *Macromolecular Symposia* 223(1), 41-56. DOI: 10.1002/masy.200550503

Hao, X., Li, Y., Wang, J., Qin, Y., and Zhang, J. (2019). "Adsorption and desorption of cellulases on/from lignin-rich residues from corn stover," *Industrial Crops and Products* 139, article ID 111559. DOI: 10.1016/j.indcrop.2019.111559

Hettrich, K., Pinnow, M., Volkert, B., Passauer, L., and Fischer, S. (2014). "Novel aspects of nanocellulose," *Cellulose* 21, 2479-2488. DOI: 10.1007/s10570-014-0265-8

Hu, F., Hu, Y., Zhang, L., Gan, M., Liu, S., Xie, Y., and Feng, Q. (2020). "Preparation and characterization of self-reinforced paper using NaOH/thiourea aqueous solution at room temperature," *BioResources* 15(4), 8191-8201. DOI: 10.15376/biores.15.4.8191-8201

Hu, Y., Hu, F., Gan, M., Xie, Y., and Feng, Q. (2021a). "A rapid, green method for the preparation of cellulosic self-reinforcing composites from wood and bamboo pulp," *Industrial Crops and Products* 169, article ID 113658. DOI: 10.1016/j.indcrop.2021.113658

Hu, Y., Hu, F., Gan, M., Xie, Y., and Feng, Q. (2021b). "Facile one-step fabrication of all cellulose composites with unique optical performance from wood and bamboo pulp," *Carbohydrate Polymers* 274, article ID 118630. DOI: 10.1016/j.carbpol.2021.118630

Jiao, L., Ma, J., and Dai, H. (2015). "Preparation and characterization of self-reinforced antibacterial and oil-resistant paper using a NaOH/urea/ZnO solution," *PLOS One* 10(10), article e0140603. DOI: 10.1371/journal.pone.0140603

Labidi, K., Korhonen, O., Zrida, M., Hamzaoui, A. H., and Budtova, T. (2019). "All-cellulose composites from alfa and wood fibers," *Industrial Crops and Products* 127, 135-141. DOI: 10.1016/j.indcrop.2018.10.055

Lee, C. M., Mittal, A., Barnette, A. L., Kafle, K., Park, Y. B., Shin, H., Johnson, D. K., Park, S., and Kim, S. H. (2013). "Cellulose polymorphism study with sum-frequency-generation (SFG) vibration spectroscopy: Identification of exocyclic CH_2OH conformation and chain orientation," *Cellulose* 20, 991-1000. DOI: 10.1007/s10570-013-9917-3

Li, T., Chen, C., Brozena, A. H., Zhu, J. Y., Xu, L., Driemeier, C., Dai, C., Rojas, O. J., Isogai, A., Wågberg, L., *et al.* (2021). "Developing fibrillated cellulose as a sustainable technological material," *Nature* 590, 47-56. DOI: 10.1038/s41586-020-03167-7

Lourdin, D., Peixinho, J., Bréard, J., Cathala, B., Leroy, E., and Duchemin, B. (2015). "Concentration driven cocrystallisation and percolation in all-cellulose nanocomposites," *Cellulose* 23, 529-543. DOI: 10.1007/s10570-015-0805-x

Ma, J., Zhu, W., Min, D., Wang, Z., and Zhou, X. (2016). "Preparation of antibacterial self-reinforced zinc oxide-cellulose composite by the synthesis of ZnO in partially dissolved cellulose," *Cellulose* 23, 3199-3208. DOI: 10.1007/s10570-016-0999-6

Montoya-Rojo, U., Alvarez-Lopez, C., and Ganan-Rojo, P. (2021). "All-cellulose composites prepared by partial dissolving of cellulose fibers from Musaceae leaf-sheath waste," *Journal of Composite Materials* 55(22), 3141-3149. DOI: 10.1177/00219983211006886

Nemoto, J., and Nakamata, K. (2021). "All-cellulose material prepared using aqueous zinc chloride solution," *Cellulose* 29, 2795-2803. DOI: 10.1007/s10570-021-04344-1

Nelson, M. L., and O'Connor, R. T. (1964a). "Relation of certain infrared bands to cellulose crystallinity and crystal lattice type. Part II. A new infrared ratio for estimation of crystallinity in celluloses I and II," *Journal of Applied Polymer Science* 8(3), 1325-1341. DOI: 10.1002/app.1964.070080323

Nelson, M. L., and O'Connor, R. T. (1964b). "Relation of certain infrared bands to cellulose crystallinity and crystal latticed type. Part I. Spectra of lattice types I, II, III

and of amorphous cellulose," *Journal of Applied Polymer Science* 8(3), 1311-1324. DOI: 10.1002/app.1964.070080322

Oh, S. Y., Yoo, D. I., Shin, Y., Kim, H. C., Kim, H. Y., Chung, Y. S., Park, W. H., and Youk, J. H. (2005). "Crystalline structure analysis of cellulose treated with sodium hydroxide and carbon dioxide by means of X-ray diffraction and FTIR spectroscopy," *Carbohydrate Research* 340(15), 2376-2391. DOI: 10.1016/j.carres.2005.08.007

Pullawan, T., Wilkinson, A. N., Zhang, L. N., and Eichhorn, S. J. (2014). "Deformation micromechanics of all-cellulose nanocomposites: Comparing matrix and reinforcing components," *Carbohydrate Polymers* 100, 31-39. DOI: 10.1016/j.carbpol.2012.12.066

Reyes, G., Aguayo, M. G., Perez, A. F., Paakkonen T., Gacitua W., and Rojas, O. J. (2019). "Dissolution and hydrolysis of bleached kraft pulp using ionic liquids," *Polymers* 11(4), article 673. DOI: 10.3390/polym11040673

Rosenau, T., Potthast, A., Sixta, H., and Kosma, P. (2001). "The chemistry of side reactions and byproduct formation in the system NMMO/cellulose (Lyocell process)," *Progress in Polymer Science* 26(9), 1763-1837. DOI: 10.1016/S0079-6700(01)00023-5

Schenzel, K., and Fischer, S. (2001). "NIR FT Raman spectroscopy – A rapid analytical tool for detecting the transformation of cellulose polymorphs," *Cellulose* 8, 49-57. DOI: 10.1023/A:1016616920539

Schenzel, K., Fischer, S., and Brendler, E. (2005). "New method for determining the degree of cellulose I crystallinity by means of FT Raman spectroscopy," *Cellulose* 12, 223-231. DOI: 10.1007/s10570-004-3885-6

Sebe, G., Ham-Pichavant, F., Ibarboure, E., Koffi, A. L., and Tingaut, P. (2012). "Supramolecular structure characterization of cellulose II nanowhiskers produced by acid hydrolysis of cellulose I substrates," *Biomacromolecules* 13(2), 570-578. DOI: 10.1021/bm201777j

Shi, Z., Yang, Q., Kuga, S., and Matsumoto, Y. (2015). "Dissolution of wood pulp in aqueous NaOH/urea solution *via* dilute acid pretreatment," *Journal of Agricultural and Food Chemistry* 63(27), 6113-6119. DOI: 10.1021/acs.jafc.5b01714

Sirviö, J. A., Visanko, M., and Hildebrandt, N. C. (2017). "Rapid preparation of all-cellulose composites by solvent welding based on the use of aqueous solvent," *European Polymer Journal* 97, 292-298. DOI: 10.1016/j.eurpolymj.2017.10.021

Tang, X., Liu, G., Zhang, H., Gao, X., Li, M., and Zhang, S. (2021). "Facile preparation of all-cellulose composites from softwood, hardwood, and agricultural straw cellulose by a simple route of partial dissolution," *Carbohydrate Polymers* 256(2021), article ID 117591. DOI: 10.1016/j.carbpol.2020.117591

Wang, Y., Yuan, L., Tian, H., Zhang, L., and Lu, A. (2019). "Strong, transparent cellulose film as gas barrier constructed *via* water evaporation induced dense packing," *Journal of Membrane Science* 585, 99-108. DOI: 10.1016/j.memsci.2019.04.059

Xi, J., Jiang, S., Lou, Y., Dai, H., and Wu, W. (2021). "Underwater superoleophobic all-cellulose composite papers for the separation of emulsified oil," *Cellulose* 28, 4357-4370. DOI: 10.1007/s10570-021-03768-z

Xia, Q., Chen, C., Yao, Y., Li, J., He, S., Zhou, Y., Li, T., Pa, X., Yao, Y., and Hu, L. (2021). "A strong, biodegradable and recyclable lignocellulosic bioplastic," *Nature Sustainability* 4, 627-635. DOI: 10.1038/s41893-021-00702-w

Xie, J., Xu, J., Cheng, Z., Chen, J., Zhang, Z., Chen, T., Yang, R., and Sheng, J. (2020). "Facile synthesis of fluorine-free cellulosic paper with excellent oil and grease resistance," *Cellulose* 27, 7009-7022. DOI: 10.1007/s10570-020-03248-w

Xiong, B., Zhao, P., Hu, K., Zhang, L., and Cheng, G. (2014), "Dissolution of cellulose in aqueous NaOH/urea solution: role of urea," *Cellulose* 21, 183-1192. DOI: 10.1007/s10570-014-0221-7

Yousefi, H., Mashkour, M., and Yousefi, R. (2015). "Direct solvent nanowelding of cellulose fibers to make all-cellulose nanocomposite," *Cellulose* 22, 1189-1200. DOI: 10.1007/s10570-015-0579-1

Yu, S., Gan, M., Chen, Y., Hu, Z., Xie, Y., and Feng, Q. (2022). "Fabrication of lignin-containing cellulose bio-composite based on unbleached corncob and wheat straw pulp," *International Journal of Biological Macromolecules* 208, 741-747. DOI: 10.1016/j.ijbiomac.2022.03.192

Zhao, D., Pang, B., Zhu, Y., Cheng, W., Cao, K., Ye, D., Si, C., Xu, G., Chen, C., and Yu, H. (2022). "A Stiffness-switchable, biomimetic smart material enabled by supramolecular reconfiguration," *Advanced Materials* 34(10), article ID 2107857. DOI: 10.1002/adma.202107857

Zhao, J., He, X., Wang, Y., Zhang, W., Zhang, X., Zhang, X., Deng, Y., and Lu, C. (2014). "Reinforcement of all-cellulose nanocomposite films using native cellulose nanofibrils," *Carbohydrate Polymers* 104, 143-150. DOI: 10.1016/j.carbpol.2014.01.007

Zhu, M., Wang, Y., Zhu, S., Xu, L., Jia, C., Dai, J., Song, J., Yao, Y., Wang, Y., Li, Y., *et al.* (2017). "Anisotropic, transparent films with aligned cellulose nanofibers," *Advanced materials* 29(21), article ID 1606284. DOI: 10.1002/adma.201606284

Article submitted: January 13, 2023; Peer review completed: February 18, 2023; Revised version received and accepted: February 26, 2023; Published: March 6, 2023.
DOI: 10.15376/biores.18.2.3044-3055